Electron-spin-resonance analysis of the natural intrinsic *EX* center in thermal SiO_2 on Si

A. Stesmans and F. Scheerlinck
Department of Physics, Katholieke Universiteit Leuven, 3001 Leuven, Belgium
(Received 24 May 1994; revised manuscript received 5 October 1994)

An electron-spin-resonance (ESR) analysis of the natural *EX* defect in thermal SiO_2 on Si is presented. Its ESR spectrum consists of a central line amid a doublet of 16.1-G splitting. The Voigt shape of the central line is deconvoluted into a Lorentzian part originating from dipole-dipole interaction, and a residual Gaussian part, likely inhomogeneously broadened due to unresolved hyperfine interaction and/or a spread in the defect's *g* factor. The 16.1-G doublet is found to arise from the ^{29}Si hyperfine interaction of the unpaired spin with three-or four equivalent Si sites, at first- or higher-order nearest-neighbor positions. The saturation behavior as well as the temperature (T) dependence of various ESR parameters of the *EX* signal are investigated: g and ΔB_{pp} are found to be T independent in the range 4.3–77 K, while the behavior of the *EX* susceptibility indicates a weak ferromagnetic coupling at low T. It is outlined that the *EX* defect is not related to any known class of defects in a-SiO_2, including P_b, E', the oxygen hole centers, and the self-trapped holes, nor can it be correlated with overcoordinated or undercoordinated O atoms. A preliminary model pictures *EX* as an unpaired electron delocalized over several atomic sites.

I. INTRODUCTION

The manufacturing of semiconductor devices, such as all types of metal-insulator-semiconductor field-effect transistors, requires high-quality insulating layers that must meet strict electrical, chemical, and mechanical demands. Amorphous silicon dioxide (a-SiO_2) has long been recognized as satisfying most of these requirements for the Si-based semiconductor device industry, explaining the unsurpassed success of the Si/SiO_2 structure. While the application boom has constantly been backed up by intense research, however, the technological race over the last 20 years toward ever smaller devices with reducing gate oxide thickness (entering the sub 100-Å region) has made the quest for quantitative fundamental understanding of basic circuits to atomic detail more important than ever. A large share of this research has been dedicated to the analysis of defects—to be seen in a broad sense—in the Si/SiO_2 structure and their often devastating impact on proper device operation and lifetime through their charge trapping nature. Hence, defect characterization in an essential part of Si/SiO_2 research.

Owing to its specific sensitivity to the physical structure of atomic defects, as sensed through the interaction of the unpaired electron, the electron-spin-resonance (ESR) technique has emerged as a most useful tool when it comes to structural identification of defects in atomic detail in solids. A major achievement of the combined effort of ESR in conjunction with theoretical calculations was the early identification[1–5] of three intrinsic E' variants in a-SiO_2: E'_α, E'_β, and E'_γ, all implying as a common entity a dangling tetrahedral orbital mainly localized on a single silicon-atom backbonded to three network oxygen atoms. As to the Si/SiO_2 entity, ESR analysis has elucidated the $P_b^{[111]}$ defect—a $Si_3\equiv Si^\bullet$ entity—at the (111)Si/SiO_2 interface.[6–13]

Until recently, the P_b centers at the Si/SiO_2 interface [the single P_b center in (111)Si/SiO_2 and the P_{b0} and P_{b1} centers in (001)Si/SiO_2] were the only *natural* (i.e., observed in as-grown samples) intrinsic defects in this structure observed by ESR. This situation, however, has recently changed through the ESR report[14] of a "new"[15] natural intrinsic defect—denoted as the *EX* center—in as-grown thermal SiO_2 on (111)Si.

The generation aspects of this defect were extensively described elsewhere.[16] In short, the *EX* center has been observed by ESR in Si/SiO_2 structures grown at oxidation temperatures (T_{ox}) from 700 up to 930 °C. The defect was encountered both in (111)Si/SiO_2 and (001)Si/SiO_2 in nearly identical areal densities (N_A^{EX}), where the spin density observed in the as-oxidized state could be significantly enhanced through a postoxidation vacuum treatment (dehydrogenation). Subsequent investigation of the hydrogen involvement through alternated annealing in vacuum and molecular hydrogen at various temperatures showed the defect's thermochemical properties to be dominated by the interaction with hydrogen, in a very similar way as is the case for P_b center at the (111)Si/SiO_2 interface: The *EX* center is readily passivated in H_2 at 360 °C (anneal time $t_{an}\approx 20$ min)—a process assumed to result in a neutral defect symbolized as H*EX*—while H is liberated from the defect sites (rendering them ESR active again) upon degassing in vacuum (pressure $p \lesssim 3\times 10^{-5}$ Pa) at $T \gtrsim 550$ °C ($t_{an}\approx 1$ h). It was further observed that *EX* generation is sensitive to the surface condition of the c-Si substrate after the prethermal cleaning treatment: After a sacrificial oxidation [the oxide being removed in a 4% aqueous hydrogen fluoride (HF) solution], these HF-cleaned surfaces, which are predominantly H terminated,[17] resulted in a 4–5-times-larger *EX* density than RCA (Radio Corporation of America; see, e.g., Ref. 18) precleaned samples. The latter, as known, leaves the substrate covered with a thin (≈ 13 Å) chemical oxide.[18]

For a fixed Si surface condition, however, the main re-

0163-1829/95/51(8)/4987(11)/$06.00 ©1995 The American Physical Society

sult of varying the oxidation parameters, such as T_{ox}, oxidation time (t_{ox}), and oxygen pressure (p_{O_2}), was that the *EX* density is *solely* determined by the grown oxide *thickness* (d_{ox}). Indeed, *EX* data obtained on (111) and (001) Si/SiO_2 grown at various T_{ox}, t_{ox}, and p_{O_2} could be unified in a single N_A^{EX} versus d_{ox} curve, with the ESR-active defect density (in terms of electron spin $S=\frac{1}{2}$ centers of a Si:P marker; *vide infra)* peaking at $(1.2\pm0.1)\times10^{12}$ cm^{-2} for $d_{ox}\approx125$ Å (see Fig. 6 in Ref. 16). The centers could be traced by ESR from $d_{ox}\approx100$ Å onwards, N_A^{EX} increasing steeply for $d_{ox}\to125$ Å; while for $d_{ox}>125$ Å, the density declines slowly eventually reaching zero for large d_{ox}, e.g., $N_A^{EX}\to5\times10^{10}$ cm^{-2} for $d_{ox}\approx217$ Å. The *EX* defects were found[16] to reside in the top ~40 Å of the oxide layer, the largest local volume densities (a few times 10^{18} cm^{-3}) occurring near the SiO_2/ambient interface. The *EX* distribution is found to be well described by a hemi-Gaussian curve of standard deviation $\sigma=14\pm2$ Å centered at the free SiO_2 surface. This particular *EX* location and *EX* density, peaking for thin SiO_2 films, might suggest the *EX* defect to be some fossile relic of the interface.

The perforce provisional conclusion from the analysis of all growth aspects suggested *EX* to be an O-rich defect of which the generation kinetics are governed by the O_2 abundance at the SiO_2/O_2 border, in intricate interplay with structural relaxation of the oxide. In an attempt to narrow down this vague description regarding the atomic nature of the *EX* center, we now address ESR properties in detail, and compare the ESR data with those of other (known) centers in *a*-SiO_2.

II. EXPERIMENTAL PROCEDURES

The studied sets of samples of both (001) and (111) thermal Si/SiO_2, grown on *p*-type Si slices at various oxidation temperatures (700–930 °C), were the same as those used in a previous study of the *EX* growth aspects.[16] Thin (50–200 Å) dry thermal oxides were grown on HF precleaned Si substrates and subsequently dehydrogenated in a conventional furnace[8] along the lines described in Ref. 16.

ESR experiments were carried out mainly at 4.3 K in a *K*-band (≈20.2 GHz) spectrometer. (See Ref. 19 for more details on spectrometer build up and performance.) The amplitude of the modulation superposed on the applied magnetic induction **B** and the incident microwave power P_μ were always sufficiently reduced to avoid overmodulation and saturation distortion. Areal spin densities were determined relative to a Si:P reference sample[20] of known spin content by double numerical integration of the respective derivative absorption spectra. This reference sample of $g(4.3\text{ K})=1.998\,69\pm0.000\,02$ served at the same time as a *g* marker.

III. RESULTS AND INTERPRETATION

A. Main features of the *EX* spectrum

As mentioned, the ESR-active *EX* areal density appears solely determined by the grown oxide thickness: In both (111) and (001)Si/SiO_2, nearly identical maximum spin densities of about $(1.1-1.2)\times10^{12}$ cm^{-2} were measured for $d_{ox}\approx125$ Å. Samples were grown in 110-kPa dry O_2 (99.999% pure) at 800 °C for t_{ox} adjusted to reach $d_{ox}\approx125$ Å [$t_{ox}\approx130$ and ≈225 min for the (111) and (001) samples, respectively], and subsequently exhaustively dehydrogenated. *EX* spectra of these samples containing the maximum defect density are shown in Fig. 1. Both spectra were recorded at 4.3 K, with φ_B (the angle between **B** and the normal to the Si/SiO_2 interface)=75° and 0°, respectively.[21] This figure illustrates two typical ESR features.

First, the (111) and (001) spectra both exhibit a narrow symmetric central signal (labeled *EX*) at $g=2.002\,46\pm0.000\,03$, with a linewidth of about 1.1 G for $N_A^{EX}=(1.2\pm0.1)\times10^{12}$ cm^{-2} and $(1.1\pm0.1)\times10^{12}$ cm^{-2} in the (111) and (001) samples, respectively. Second, the central line situates amid a weak symmetric doublet (labeled *d*) of 16.1-G splitting and averaged intensity ratio $R=I_d/I_c=0.14\pm0.02$ [I_d and I_c being the integrated intensity (area under absorption curve) of the doublet lines

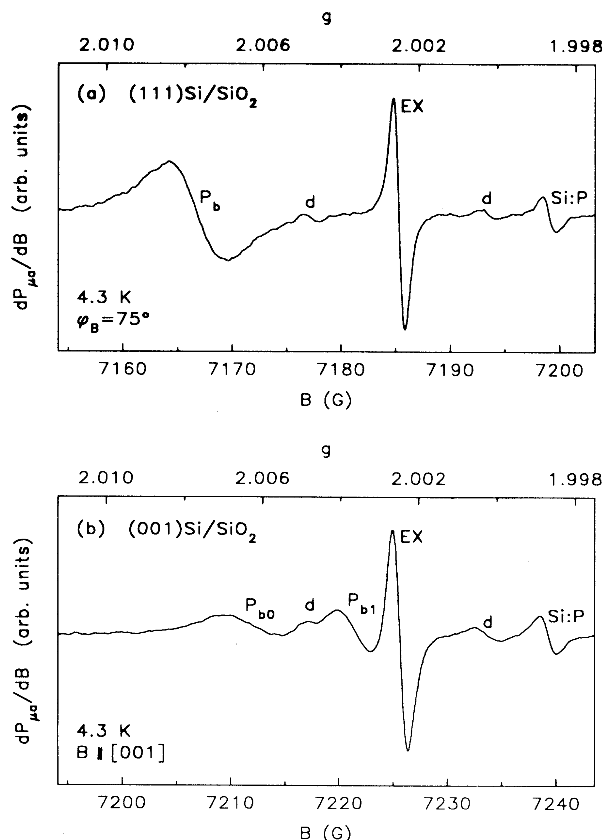

FIG. 1. *K*-band first-derivative absorption spectra obtained at 4.3 K on (a) (111)Si/SiO_2 and (b) (001)Si/SiO_2 grown at 800 °C for 130 and 225 min, respectively, in 110-kPa dry O_2 and subsequently vacuum treated at 790 °C for ≈1 h. The narrow symmetric *EX* signal at $g=2.002\,46$ is accompanied by a symmetric doublet of 16.1-G splitting (labeled *d*) centered at the central line. The signal denoted as Si:P stems from a Si:P reference sample of $g(4.3\text{ K})=1.998\,69$. The signals labeled P_b, P_{b0}, and P_{b1} originate from the unpaired bond defects at the (111) and (001)Si/SiO_2 interface, respectively.

and central line, respectively], both for (111) and (001)Si/SiO_2. The linewidth of each doublet line is about 1.2 G, i.e., comparable to the central-signal's width. No other satellites could be found, although an extensive search was conducted, using signal averaging, in a magnetic-field window of 1000 G centered at the *EX* central line. The spectral composition refers to an $S=\frac{1}{2}$ center. The remaining resonance lines in Fig. 1 originate from P_b centers at the Si/SiO_2 interface, i.e., the line labeled P_b in Fig. 1(a) and the lines labeled P_{b0} and P_{b1} in Fig. 1(b).

B. The central *EX* signal

1. *Symmetry and g value*

As expected for a spin system residing in an amorphous network, no *g* anisotropy is observed within experimental error (see Fig. 2). However, more specific information regarding the defect's individual *g* matrix symmetry comes from the spiral shape. A basic feature of the *EX* central line is its symmetric paramagnetic shape. As the *EX* defects are found to reside in the top ~40 Å of the SiO_2 layer[16]—that is, a noncrystalline environment where any *g* anisotropy would show up as a powder pattern effect—this symmetry betrays a highly isotropic *g* tensor.

The next observation is that the g_{EX} value of 2.002 46±0.000 03 is larger than the free-electron value $g_0=2.002\,319$—characteristic of hole centers. This property ($g_{EX}>g_0$), in addition to the *g* matrix isotropy, makes the *EX* center well distinct from the common defects in the thermal SiO_2 structure, such as the P_b centers [$P_b^{[111]}$ in (111)Si/SiO_2: $g_{\parallel}=2.0014$, $g_{\perp}=2.0086\pm0.0003$;[9,11,16] P_{b0} and P_{b1} in (001)Si/SiO_s: $g_1=2.0015$, $g_2=2.0080$, $g_3=2.0087$, and $g_1=2.0012-2.0020$, $g_2=2.0081\pm0.0003$, $g_3=2.0052-2.0058$ (Refs. 9 and 22), respectively], and the widely studied E' centers: All *g* values of the different E' varieties are smaller than g_0.[23,24]

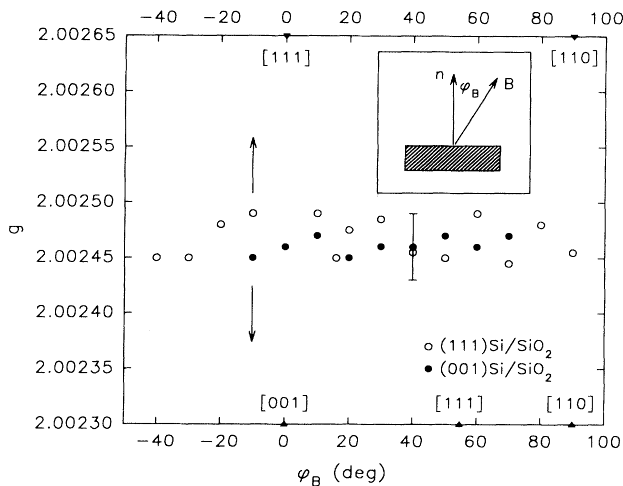

FIG. 2. *EX g* map at 4.3 K for (111)Si/SiO_2 (open circles) and (001)Si/SiO_2 (filled circles); the field angle φ_B is defined in the inset, where $\bar{n}$ denotes a vector normal to the sample surface. **B** is rotated in the $(11\bar{2})$ plane for (111)Si/SiO_2 and in the $(1\bar{1}0)$ plane for (001) samples. A typical error bar is also shown, as are the principal *c*-Si directions (filled triangles).

2. *Line shape*

The *EX* signal is generally found to exhibit the Voigt profile, which represents the convolution of Gaussian and Lorentzian broadening. In the absence of saturation effects ($S\equiv\gamma^2B_1^2T_1T_2\ll1$; γ, B_1, T_1, and T_2 being the gyromagnetic ratio, the microwave amplitude, the spin-lattice relaxation time, and the spin-spin relaxation time, respectively), it is given as[25]

$$Y(v,b)=\frac{b}{\pi}\int_{-\infty}^{+\infty}\frac{e^{-x^2}dx}{b^2+(v-x)^2}\ , \qquad (1)$$

where

$$v=\sqrt{2}(B-B_0)/\Delta B_{\rm pp}^{G}$$

and

$$b=\sqrt{3/2}(\Delta B_{\rm pp}^{L}/\Delta B_{\rm pp}^{G});$$ $\Delta B_{\rm pp}^{L}$ and $\Delta B_{\rm pp}^{G}$ are the peak-to-peak derivative widths of the Lorentzian and Gaussian components, respectively.

For a density $N_A^{EX}\approx10^{12}$ cm^{-2}, the line-shape factor $\kappa\equiv I_c/A_{\rm pp}(\Delta B_{\rm pp})^2=1.8\pm0.1$, where $2A_{\rm pp}$ and $\Delta B_{\rm pp}$ represent the peak-to-peak amplitude and linewidth, respectively. (We recall that the basic Gaussian and Lorentzian curves are characterized by $\kappa=1.03$ and 3.63, respectively. Hence, the range $1.03\le\kappa\le3.63$ applies for the Voigt shape.) The shape, and its attendant κ value, are found to be isotropic, i.e., independent of φ_B. Neither could any φ_B dependence of $\Delta B_{\rm pp}$ be traced, as shown in Fig. 3. These results add to the isotropic nature of the *EX* center.

The situation somewhat alters with varying areal *EX* density. While the line shape still remains Voigt-like throughout, $\Delta B_{\rm pp}$ is found to closely track—almost linearly—the variations in N_A^{EX}, as shown in Fig. 4. An observation relevant to this N_A^{EX}-dependent broadening is

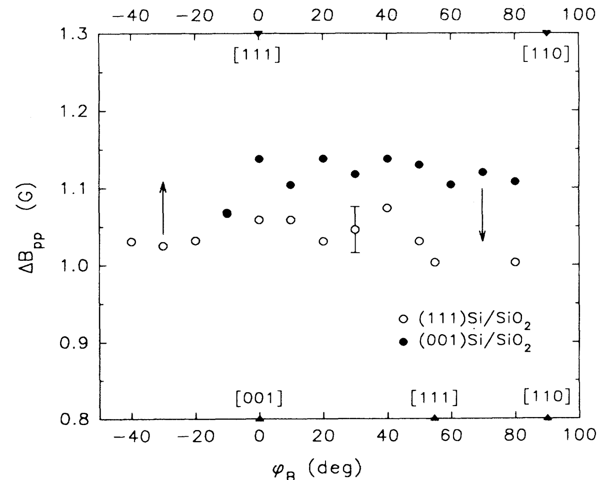

FIG. 3. Plot of the *EX* signal's peak-to-peak linewidth, measured at 4.3 K, as a function of magnetic field angle (see Fig. 2) for (111)Si/SiO_2 (open circles) and (001)Si/SiO_2 (filled circles). The (111) and (001) samples have different N_A^{EX} and, hence, different $\Delta B_{\rm pp}$ values (see text).

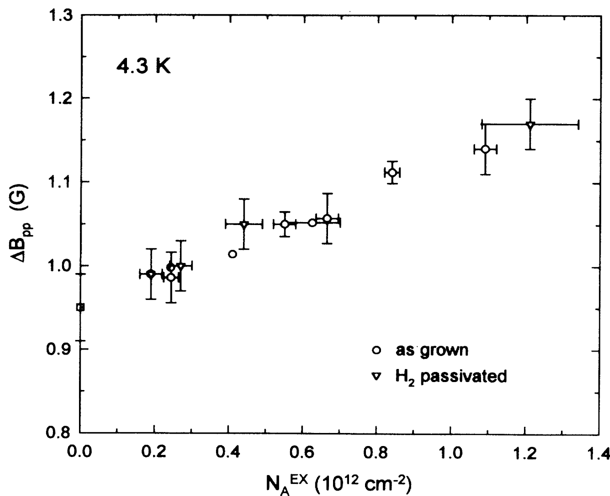

FIG. 4. Variation of the peak-to-peak linewidth of the EX first-derivative absorption signal, measured at 4.3 K, as a function of the areal ESR-active defect density. Data points are included for both (111) and (001)Si/SiO_2 samples. Unfilled circles and triangles correspond to standardly grown and partially repassivated samples, respectively (see text). Horizontal and vertical error bars represent the standard deviation over various measurements. The data point for $N_A^{EX} \rightarrow 0$ (unfilled square) is observed on a Si-powder oxidized at 800 °C for ~17 h to $d_{ox} \approx 600$ Å and subsequently exhaustively dehydrogenated at ~790 °C.

that the EX defects, regardless of the particular EX density present, are invariably located in the top ~40 Å of the SiO_2 layer. The spatial extension of the region housing the EX centers remains practically fixed. Hence, the effect of altering N_A^{EX} (realized through growing various d_{ox}) is merely mirrored as changes in the local *volume* density, revealing as the net result of Fig. 4 ΔB_{pp} to increase with reducing average spin-spin separation. This indicates that part of the total linewidth stems from dipole-dipole (DD) interaction, adding a broadening ΔB_{pp}^{DD} to the overall linewidth. The functional dependence of ΔB_{pp}^{DD} on the fractional spin population f of network sites has been well analyzed for the three-dimensional (3D) DD interaction (as is for the 2D case). In general, $\Delta B_{pp}^{DD} \propto \sqrt{f}$ in the high-f range ($f \rightarrow 1$), attendant with a closely Gaussian line shape, whereas for low f (typically $< 1\%$) the line shape evolves to a cut-off Lorentzian[26] of which $\Delta B_{pp}^{DD} \propto f$. With the EX defects confined to the top 40-Å oxide layer, it follows that $N_A^{EX} \approx 10^{12}$ cm^{-2} (~ maximum density) corresponds to an average volume density of a few times 10^{18} cm^{-3}. So, with the SiO_2 molecular density of $\sim 2.28 \times 10^{22}$ cm^{-3}, this implies that $f \ll 1\%$, and hence, for all EX densities encountered in this study, the relation $\Delta B_{pp}^{DD} \propto f$ (Ref. 26) should apply. To check this prognosis, it remains to extract ΔB_{pp}^{DD} from the linewidth data.

The EX spectra of samples with N_A^{EX} ranging from $\sim 10^{11}$ to 10^{12} cm^{-2} were fitted with Voigt functions, each obtained as the convolution of a fixed Gaussian profile (referred to as the *residual* shape) with a Lorentzian of variable linewidth ΔB_{pp}^{L} ($\equiv \Delta B_{pp}^{DD}$) reflecting the DD broadening. The residual shape was found to have a peak-to-peak width $\Delta B_{pp}^{G} = \Delta B_{pp}^{R} \approx 0.8$ G for samples oxidized at 800 °C. Typical fitting examples are depicted in Figs. 5(a) and 5(b) showing EX spectra for samples having $N_A^{EX} = 1.0 \times 10^{12}$ cm^{-2} and 0.5×10^{12} cm^{-2}, together with Voigt-like fits characterized by $\Delta B_{pp}^{G} = 0.78$ G (fixed) and $\Delta B_{pp}^{L} = 0.64$ and 0.45 G, respectively. The various ΔB_{pp}^{L} results obtained along this fitting procedure are summarized in Fig. 6, together with a linear least-squares fit to the data. Two features in this plot merit attention. First, it is observed that ΔB_{pp}^{L} does *not* extrapolate to zero for $N_A^{EX} \rightarrow 0$, but rather tends to a value of ≈ 0.28 G. Second, the $\Delta B_{pp}^{L} - N_A^{EX}$ relationship appears linear. These observations are addressed in more detail.

For N_A^{EX} below $\sim 0.2 \times 10^{12}$ cm^{-2}, the SiO_2-to-Si volume ratio that may be reached the conventional way by stacking platelets is insufficient with current ESR sensitivity to determine ΔB_{pp}^{L} reliably. Therefore, some crystalline Si was powdered to particles of ~5 μm average size and subsequently oxidized ($t_{ox} = 17$ h at 800 °C) to a large oxide thickness (≈ 600 Å), much larger than the "optimum" $d_{ox} \approx 125$ Å, with attendant strong reduction in EX volume density (for $d_{ox} \approx 217$ Å, $N_A^{EX} \approx 5 \times 10^{10}$

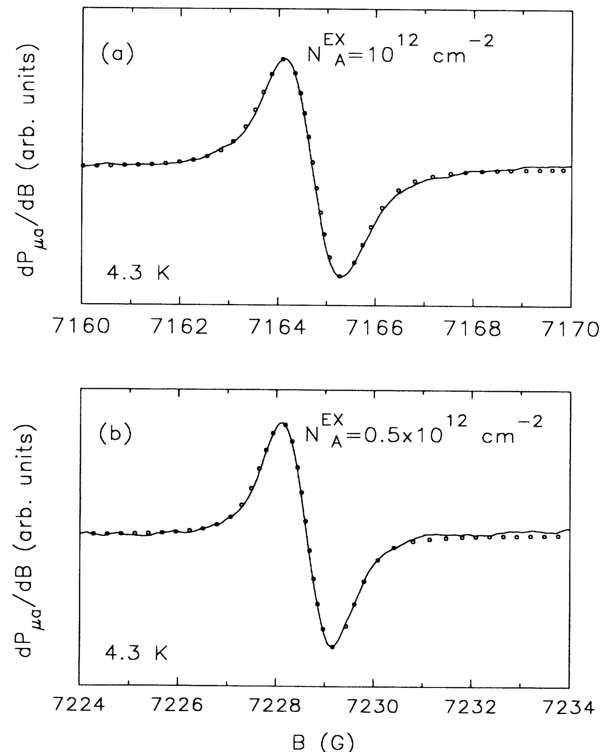

FIG. 5. First-derivative absorption profiles of the EX defect measured at 4.3 K on (a) (111)Si/SiO_2 containing $N_A^{EX} = 1.0 \times 10^{12}$ cm^{-2} and (b) (111)Si/SiO_2 of $N_A^{EX} = 0.5 \times 10^{12}$ cm^{-2}, both grown at 800 °C with $t_{ox} = 120$ and 224 min, $p_{O_2} = 110$ and 24 kPa, for (a) and (b), respectively. The open circles represent fits of the Voigt function [see Eq. (1)] to the data using $\Delta B_{pp}^{G} = 0.8$ G (kept fixed), and $\Delta B_{pp}^{L} = 0.64$ (a) and 0.45 G (b).

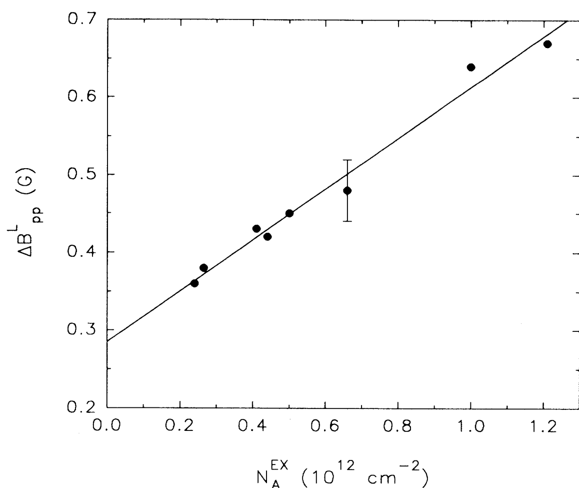

FIG. 6. Variation of the Lorentzian DD broadening as a function of the measured areal ESR-active EX density. $\Delta B^{L}_{\mathrm{pp}}$ was obtained through fitting a Voigt function [see Eq. (1)] with $\Delta B^{G}_{\mathrm{pp}}=0.8$ G to the EX derivative absorption spectra at 4.3 K, for N^{EX}_{A} ranging from $\sim 10^{11}$ to 10^{12} cm^{-2}. A typical error bar is shown for $\Delta B^{L}_{\mathrm{pp}}$, corresponding to the smallest ΔB step (± 0.04 G) used to construct the Voigt profile. The full line represents the linear least-squares fit to the data (with a regression coefficient of 0.99).

cm^{-2}). [A rough estimate of the effective sample area of the powdered samples is obtained from a straightforward calculation assuming hexagonal close packing of spherical particles of ~ 5 μm diam in the available sample space. The obtained powder sample area of ~ 540 cm^2 indicates a gain in signal-to-noise ratio of about a factor 100 as compared to the case of conventional stacking of platelets (2 mm$\times$4 mm) into a sample bundle.] The EX DD contribution is believed to be essentially negligible in this sample; yet, as illustrated in Fig. 7(a) for 870 °C powder (displaying the same features as for $T_{\mathrm{ox}}=800$ °C), the EX signal still exhibits a Voigt shape of width $\Delta B^{N}_{\mathrm{pp}}=0.97$ G (termed the *natural* width) deconvolving in Gaussian and Lorentzian linewidth contributions of ≈ 0.8 and 0.26 G, respectively. The latter value is reassuringly close to the extrapolated value of Fig. 6, from where it is concluded that $\Delta B^{L}_{\mathrm{pp}}\approx 0.26$ G for $N^{EX}_{A}\rightarrow 0$.

It remains to trace the origin of this Lorentzian contribution of 0.26 G to the natural linewidth. First, it may be stated that its origin is *not* DD interaction among EX spins, as could result, for example, from a systematic decrease of σ along with N^{EX}_{A} in the low-density region, so that the average spin-spin distance would essentially remain unaltered. While previous measurements[16] on as-grown samples already indicated σ to be largely independent of N^{EX}_{A} in the range $n^{EX}_{A}\geq 5\times 10^{10}$ cm^{-2}, this was explicitly verified here on a suite of low-N^{EX}_{A} samples obtained through stepwise partial passivation in H_2 of the EX system in *one* sample initially containing 1.2×10^{12} EX cm^{-2}. With the likely assumption that the activation energy for the EX passivation process does not exhibit a spatial dependence in the oxide, σ should remain unaltered when stepwise passivating the EX bath. As shown in Fig. 4, the linewidths measured on this stepwise passivated EX bath (triangles) coincide well with the as-grown samples data set (circles), which is counter to a systematically varying σ.

Second, this 0.26-G-wide Lorentzian cannot be the *intrinsic* line, i.e., caused by spin-lattice (T_1) relaxation. Such intrinsic width would result in $T_1\approx 4\times 10^{-7}$ s, whereas T_1 (4.3 K) ≈ 30 ms was obtained from microwave saturation data (see Sec. III D).

Third, a possibility is that it arises from DD interaction with another defect bath, of density comparable to N^{EX}_{V} and with a concentration largely constant over the studied N^{EX}_{A} range. Excessive line broadening may so far have prevented ESR detection of these defects.

With respect to Fig. 7 it is important to remark that, for $N^{EX}_{A}\rightarrow 0$ and disregarding the additional DD broadening discussed above, the signal shape evolves to a Gaussian form, rather than a Lorentzian shape. This indicates that the residual width is not the *intrinsic* width, i.e., the width $\Delta B^{\mathrm{ph}}_{\mathrm{pp}}$ caused by spin-lattice (T_1) relaxation. Likely, it is dominated by unresolved ^{29}Si (nuclear spin $I=\frac{1}{2}$; natural abundance $\zeta=4.70\%$) hyperfine (hf) broadening [for unenriched oxides the ^{17}O ($I=\frac{5}{2}$; $\zeta=0.037\%$) hf contribution is negligible] or some (weak) remnant of strain-induced g distribution (glass effect),[27] that is, inhomogeneous broadening.

There is one more interesting observation regarding

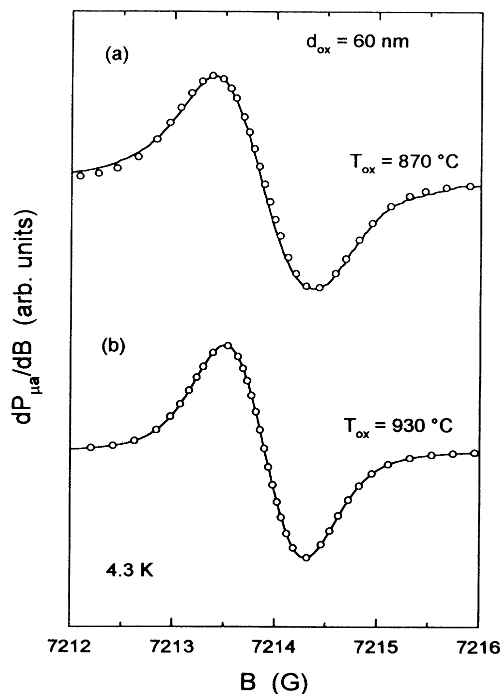

FIG. 7. K-band first-derivative absorption spectra of the EX center measured at 4.3 K on powdered Si oxidized at (a) 870 and (b) 930 °C to $d_{\mathrm{ox}}\approx 600$ Å and subsequently dehydrogenated at 790 °C for ≈ 70 min. The unfilled circles represent fits to the data with Voigt functions using $\Delta B^{L}_{\mathrm{pp}}=0.26$ G and $\Delta B^{G}_{\mathrm{pp}}=0.83$ and 0.64 G for (a) and (b), respectively.

the residual Gaussian line shape. This component is found to be *oxidation-temperature dependent* as borne out by measurements on a thick (620 Å) powder oxide grown at 930 °C (1 atm O_2, 140 min), showing a (natural) *EX* width $\Delta B^N_{pp} = 0.78 \pm 0.04$ G. Here, deconvolution reveals $\Delta B^L_{pp} = 0.26 \pm 0.04$ G and a Gaussian component of ΔB^G_{pp} (930 °C) = 0.64 ± 0.04 G [Fig. 7(b)], whereas the 800 °C oxide, as mentioned, exhibited a value $\Delta B^G_{pp} \sim 0.8$ G (cf., fits leading to the ΔB^L_{pp} values in Fig. 6). Table I summarizes the pertinent line-shape fitting results for the natural ($N^{EX}_A \to 0$) line shapes. Although the *EX* center is thermally well stable at 930 °C, this effect is ascribed to structural relaxation of the oxide, which starts playing a role in that temperature region; such cooperative rearrangement has been observed through its effect (i.e., decrease) on the intrinsic P_b density at the (111)Si/SiO_2 interface from ~850 °C onwards.[8] The rearrangement of the oxide is thus believed to result in a narrowing of the, albeit small, strain-induced g distribution at $T_{ox} = 930$ °C, hence of the inhomogeneously broadened (Gaussian) *EX* line.

The second part in the analysis of the *EX* signal shape regards the linear behavior of ΔB^L_{pp} as a function of $N^{EX}_A \propto f$. From this, we may proceed to a direct calculation of N^{EX}_V from the measured DD broadening (ΔB^L_{pp}) using the theory developed by Van Vleck,[28] and Kittel and Abrahams.[26] This theory derives that for $f < 0.01$ and magnetic centers of volume density N_V randomly distributed over a cubic lattice

$$\Delta B^L_{pp}(G) = \frac{2}{\sqrt{3}} \times 5.41 f \frac{g\beta}{d^3} = 1.16 \times 10^{-19} N_V(\text{cm}^{-3}) , \quad (2)$$

for spin $S = \frac{1}{2}$ and **B** parallel to the [001] axis of the cubic crystal; β and d are the Bohr magneton and the lattice spacing, respectively. For the case of *EX* defects, this expression is modified[29] to

$$\Delta B^L_{pp}(G) = 0.83 \times 10^{-19} N^{EX}_V(\text{cm}^{-3}) . \quad (3)$$

As an example, for $N^{EX}_A = (0.41 \pm 0.04) \times 10^{12}$ cm^{-2} the value $\Delta B^L_{pp} = 0.43$ G has been derived through curve fitting (see Fig. 6). When reducing[30] this value with the remaining Lorentzian contribution of 0.26 G for $N^{EX}_A \to 0$, which does not pertain to the intra *EX* bath DD interaction, Eq. (3) predicts a value $N^{EX}_V \approx 2.0 \times 10^{18}$ cm^{-3}, which may be compared with the measured *EX* volume density. This, however, is not straightforward given the nonuniform distribution of the *EX* centers over the top ~40-Å SiO_2 layer that they reside in. So, the DD linewidth contribution from the various "*EX* layers" may decrease with depth in the oxide. However, if accepting the hemi-Gaussian depth distribution of $\sigma \approx 16$ Å, one may define an *average* volume density $(N^{EX}_V)_{av} = N^{EX}_A / \sigma \sim 3 \times 10^{18}$ cm^{-3}, which compares favorably with the N^{EX}_V value deduced above from the dipolar broadening ΔB^{DD}_{pp}.

TABLE I. Tabulation of the *EX* linewidth deconvolution results as obtained by least-squares fitting of the Voigt function to the natural ($N^{EX}_A \to 0$) signal of width ΔB^N_{pp}, measured on oxidized Si powders of ~5-μm average particle size at 4.3 K.

T_{ox} (°C)	ΔB^N_{pp} (±0.04 G)	ΔB^L_{pp} (G)	ΔB^G_{pp} (G)	κ_{th}[a]	κ_{exp}
800	0.95	0.26	0.80		
870	0.97	0.26	0.83	1.38	1.40
930	0.78	0.26	0.64	1.44	1.52

[a]κ_{th} is determined from the fitted Voigt profile.

C. hf structure

A next step in the *EX* analysis regards the origin of the doublet signals [labeled *d* in Figs. 1(a) and 1(b)]. As the doublet is best observed at the largest N^{EX}_A, we have restricted this discussion to "optimum" samples of $d_{ox} \approx 125$ Å. The main question is whether this doublet together with the central signal constitute the complete ESR spectrum of one type of defect, where it may then concern either hf or fine structure. Or, along a more extreme interpretation, does it simply constitute the ESR spectrum of a different defect (that is, not related with the central signal), the two-peak structure resulting from the hf interaction of the unpaired electron with a $I = \frac{1}{2}$ isotope of 100% natural abundance. Hence, the spectral composition by itself is generally insufficient to make a correct assignment; additional information must be invoked, such as the dependence of the spectrum on the concentration of suspected atoms, defect concentration influence, line shapes, g values, etc.

The synthesis of this is that various facts hint in the direction of a hf doublet pertaining to the central line, i.e., the *EX* defect: (1) The doublet lines, like the central peak, are also found to be symmetric. (2) The doublet g value coincides, within experimental accuracy, with the central-peak g value, and, like the latter, is also isotropic. (3) The width of the doublet lines, for $N^{EX}_A \sim 10^{12}$ cm^{-2}, is ≈ 1.2 G, that is, slightly broader than the central peak; such an effect is generally observed in a glassy or strained surrounding, leading to slight variations in the defect's structure from site to site, with attendant site-dependent weak alterations in the distribution of the unpaired electron's wave function ψ_s. (4) The ratio of the doublet to central-line intensities appears constant, i.e., independent of N^{EX}_A and T. The sum of these properties identify the doublets as *EX* hf structure.

The next level of identification then should clarify whether it concerns a hf doublet in due sense, that is, originating from a $I = \frac{1}{2}$ species, or instead, whether it is merely the prominent part of a $I > \frac{1}{2}$ multiplet, where in the case of $I > 1$, the outer lines might have remained undetectable due to limited sensitivity. However, the latter possibility is considered unlikely in light of the thorough search for additional structure that remained unsuccessful and the expected signal-to-noise ratio (SN) (as estimated from the SN ratio of the observed doublet) for the additional lines in a $2I+1$ peaks spectrum. This, importantly, would exclude the ^{17}O and ^{11}B [$I = \frac{3}{2}$: $\zeta = 80.22\%$ (Ref. 31)] isotopes as possible candidates. But the discrimination between the $I = \frac{1}{2}$ and the $I = 1$ possibilities requires more care. Indeed, instead of being a simple

$I=\frac{1}{2}$ hf structure, the doublet might just constitute the outer lines of an $I=1$ triplet resulting from interaction of the unpaired electron spin with the nucleus of an atomic species of which both $I=0$ and $I=1$ isotopes are naturally abundant in appropriate amounts. The third, central hf peak will then have merged with the $I=0$ isotope signal. Along the latter suggestion, the *EX* spectrum might well correspond to hf interaction with an atomic species typified by an isotopic abundance ratio $R_i \equiv [I=1$ isotopes]/[$I=0$ isotopes] $=0.187/0.813 \approx 0.23$. Hence, it follows that, in terms of ESR spectroscopy, the final identification of the interacting nuclear spin would require isotope substitution experiments.[32] However, the $I=1$ possibility can be discarded on different grounds, as no atomic species exhibiting $R_i=0.23$ is likely to occur in sufficient amounts in the Si/SiO_2 structure. A particularly interesting corollary of this analysis is that the one-atom-site ^{14}N ($I=1$; $\zeta=99.63\%$) hf interaction can be ruled out as the origin of the *EX* spectral structure.

This brings us to assigning the *EX* hf structure to an $I=\frac{1}{2}$ hf interaction. For an intrinsic deffect in a-SiO_2, this would, in principle, only leave ^{29}Si as a candidate if it weren't for the fact that other nuclear $I=\frac{1}{2}$ isotopes, such as ^{1}H, may also get incorporated in a-SiO_2 in nonnegligible amounts. Thus, we list in Table II common $I=\frac{1}{2}$ nuclei encountered in Si/SiO_2 after processing, together with the expected R values as calculated starting from simple binomial probabilities ("stick" diagrams). For each isotope is considered a possible interaction of the unpaired electron with n equivalent atomic sites, n running from 1 to 6. In each case then, the intensity of the strongest hf pair centered at the central resonance field was taken to calculate the tabulated theoretical R. The strongest hf lines have to be chosen because we do not observe hf signals other than the 16.1-G doublet in the *EX* spectrum. The values in Table II may be compared with the experimental value [determined on both (111) and (001)Si/SiO_2] $R=0.14\pm0.02$. It is clear that we can immediately exclude all $I=\frac{1}{2}$ isotopes other than ^{29}Si, which implicitly seems to exclude an impurity-related origin for the *EX* center (see Sec. IV).

Generally, two parameters of this hf spectrum, in combination with simple localized hybrid orbital calculations, may provide key information on the defect's atomic structure and its immediate surroundings. These are the magnitude of the hf splitting a and the intensity ratio R. In the course of mapping g_{EX} versus φ_B, it was observed that the hf tensor, like the g dyadic, is also isotropic, that is, $a_\perp = a_\parallel \equiv a = 16.1$ G. This implies that the hf interaction giving rise to the doublet is either entirely dominated by the Fermi-contact interaction, reflecting the probability of finding the unpaired spin at the site of the magnetic nuclei, or that the anisotropic part of the hf interaction, arising from DD interaction between the defect and nuclear spin(s), is averaged out.

While the magnitude of the hf splitting may provide an idea of the localization of the unpaired-electron wave function with respect to the magnetic nuclei (in a sense to be explained below), the R value, once the nuclear spin I is ascertained, carries information on the number of equivalent atomic sites the spin interacts with. Because of the defect's isotropy and the isotropy of the hf tensor, the hf doublet originates from interaction of the defect spin with a number of nuclei in equivalent sites, whose arrangement reflects the observed spherical symmetry.

It is seen in the ^{29}Si column of Table II that the underlined theoretical value of 0.1475 comes closest to the experimental value, indicating that the *EX* spin interacts with three equivalent Si sites. We should add, though, that it has been found in previous work dealing with the ^{29}Si hf structure of the P_b center that the measured R value can be somewhat lower than the theoretically predicted value, due to broadened portions of the hf structure lost in noise.[10] The presently measured R value may, therefore, perhaps not totally exclude interaction with more than three equivalent Si sites.

It is important to add that the possibility of the *EX* unpaired orbital being *primarily* located on three (maybe four) equivalent Si sites has to be excluded when considering the magnitude of a: a pure Si 3s orbital would give rise to a hf splitting of ≈ 1220 G,[34] indicating that the equivalent Si sites must be first- or higher-order nearest neighbors, and that the observed doublet originates from superhyperfine interaction.

Finally then, there remains the question as to the na-

TABLE II. Theoretical ratio R of the hyperfine to the central-line intensity for an unpaired electron interacting with n equivalent neighboring nuclei of spin $I=\frac{1}{2}$ ($n=1-6$) for the common species encountered in Si/SiO_2 after processing. The underlined figure is closest to the experimentally determined value of 0.14 ± 0.02.

	ISOTOPE Natural abundance[a] (%)						
	^{1}H	^{13}C	^{13}N	^{15}N	^{19}F	^{29}Si	^{31}P
	99.985	1.11	0.01	0.37	100	4.70	100
$n=1$	6665.7	0.0112	0.0001	0.0037	$+\infty$[b]	0.0493	$+\infty$
$n=2$	0.9999	0.0224	0.0002	0.0074	1.0000	0.0985	1.0000
$n=3$	3331.6	0.0337	0.0003	0.0111	$+\infty$	$\underline{0.1475}$	$+\infty$
$n=4$	1.3333	0.0449	0.0004	0.0149	1.3333	0.1962	1.333
$n=5$	2221.6	0.0561	0.0005	0.0186	$+\infty$	0.2445	$+\infty$
$n=6$	1.5000	0.0673	0.0006	0.0223	1.5000	0.2924	1.5000

[a]See Ref. 31.

[b]$R=+\infty$ means that the initial central line is completely split out into the hf lines.

ture of the *EX* defect's core atom(s). It is possible that these atomic species do not possess a magnetic isotope in any substantial amount to give rise to other observable hf lines or, alternatively, the hf splitting due to the *EX* core atoms might be too large (and the hf lines too broad) to be detectable. The hf structure due to higher-order nearest neighbors (further away than the three or four equivalent Si sites), on the other hand, is likely not resolved in the *EX* central line (see Sec. III B).

D. Saturation and thermal stability

The ESR saturability is another parameter that may contribute to the identification of defects. The saturability of the central *EX* signal has been compared to that of the copresent natural intrinsic P_b signal and an E' signal. Continuous-wave saturation curves of these three defects were measured simultaneously by some crushed HSQ200-type fused quartz[35] ([OH] < 30 ppm, [other impurities] < 20 ppm) next to a (111)Si/SiO_2 sample ($T_{ox} = 800\,°C$, $t_{ox} = 106$ min, $d_{ox} \approx 115$ Å) into the spectrometer cavity. The derivative amplitude A_{pp} (normalized in the nonsaturation regime, i.e., $B_1 < 10^{-4}$ G) of each defect signal is plotted in Fig. 8 as a function of B_1 at the sample site [determined from the incident power P_μ and the quality factor (Q)]. The data, measured at 4.3 K with $\mathbf{B} \parallel \langle 111 \rangle$ surface, show that the three types of defects exhibit a distinctly different relaxation behavior, the *EX* saturation characteristics neither matching those of the E' nor P_b defects. While this would suggest that the *EX* center does not belong to either type of defect family, it does not constitute conclusive proof, however: The local defect density does affect the spin-spin relaxation time T_2 through DD interaction and, as the saturation characteristics are governed by the product $T_1 T_2$

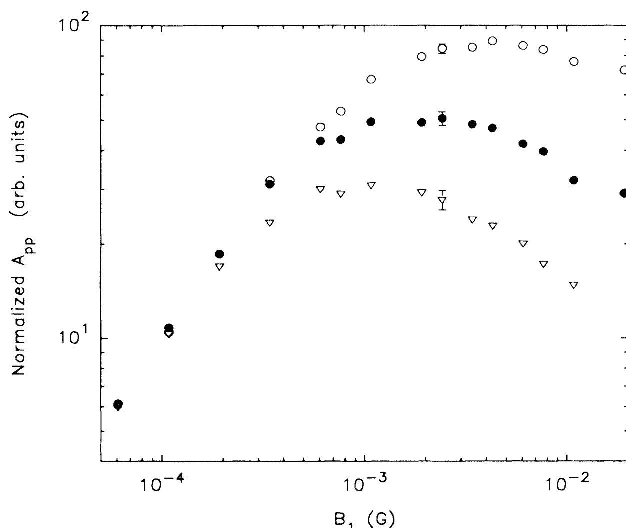

FIG. 8. Continuous-wave saturation curves measured at 4.3 K. The P_b, *EX*, and E' data are represented by unfilled circles, filled circles, and unfilled triangles, respectively. The data are normalized in the nonsaturation regime. The *EX* and P_b signals are observed on a (111)Si/SiO_2 sample, while the E' signal stems from crushed fused quartz.

(see, e.g., Ref. 36), the particular saturation behavior will depend on the defect's volume concentration, even when the spin-lattice relaxation time (T_1) remains unchanged. From the maximum of the *EX* saturation curve in Fig. 8 (where $\gamma^2 B_1^2 T_1 T_2 \approx$ according to theory), $T_1(4.3\text{ K}) \approx 30$ ms is inferred, comparable with the T_1 value of a P_b bath at 4.3 K.

A next series of experiments could aim to map isochronal anneal curves *in vacuo* in order to further characterize the *EX* defect. As outlined, however, the *EX* defect bath in a Si/SiO_2 sample, once properly dehydrogenated, remains unaffected by prolonged annealing in vacuum up to 930 °C: no variation in *EX* density is observed. This is in contrast with the isochronal annealing behavior—the gradual decrease of defect density with stepwise increasing T_{an}—of the various identified *damage* centers in SiO_2, which is taken as a fingerprint for each particular defect.[23,24] All damage defects, such as the oxygen hole center, the peroxy radical, and the various E' variants—though distinct differently—are seen to gradually anneal out in the range 100–930 °C. This, again, underlines the different nature of the *EX* centers as compared to the well-known defects, i.e., a *natural* (grown in) defect *vis-á-vis damage-induced* centers. The latter, apparently, may gradually get repaired by thermal energy, while natural defects are fixed by the specific network arrangement.

E. Temperature dependence of the *EX* resonance

The temperature dependence of the *EX* signal was studied over the range 4.3–77 K on a (111)Si/SiO_2 sample (effective sample surface $\approx 10\text{ cm}^2$) grown at 800 °C in 110-kPa dry O_2 for $t_{ox} \approx 133$ min. The initial *EX* density at 4.3 K was $\sim 0.6 \times 10^{12}\text{ cm}^{-2}$. Above 77 K, the cavity Q, and hence the spectral quality too, gets severely degraded although the *EX* resonance remains detectable up to room temperature.

The plots of g_{EX} and ΔB_{pp} versus temperature, shown in Fig. 9, do not bear out a systemic T dependence. Of particular interest, however, is the T dependence of the *EX* susceptibility χ_{EX}. For a sufficiently diluted system of spins embedded in an insulating matrix, one would normally expect a Curie-type behavior ($\chi \propto N_V^{EX}/T$). But before addressing this $\chi_{EX} - T$ relationship, it needs to be remarked that, rather than χ_{EX}, the areal spin density N_A^{EX} is derived at each observational temperature in terms of the number of marker spins N_m, along the expression

$$N_A^{EX} = \frac{I_{EX}(T)}{I_m(T)} \frac{\eta}{A} \frac{N_m}{C} . \tag{4}$$

Here, $I_{EX}(T)$ and $I_m(T)$ represent the (temperature-dependent) integrated intensities of the *EX* signal and the Si:P marker signal, respectively; η is a geometrical factor and A the effective sample area; $C = [(T - \Theta_m)/T]$ represents a correction factor accounting for the antiferromagnetic coupling of the marker spins, their susceptibility being described by $\chi_m \propto N_V^m/(T - \Theta_m)$, with $\Theta_m = -2.7 \pm 0.3$ K. Including this correction factor in Eq. (4) effectively transforms the $\chi_m - T$ relationship to a perfect Curie-like behavior (i.e., $\chi_m \propto T^{-1}$). Should the

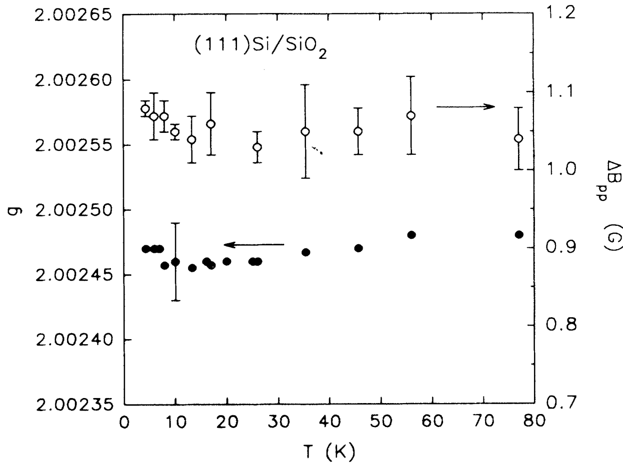

FIG. 9. Temperature dependence of g (filled circles) and ΔB_{pp} (unfilled circles) for (111)Si/SiO_2 grown at 800 °C in 110-kPa dry O_2 for ≈ 133 min. The error bars are obtained from statistical averaging over various spectra recorded at each observational temperature.

susceptibility of the measured spin system—EX defects in this case—also exhibit the ideal Curie-like behavior, then a constant N_A^{EX} value will be obtained at each observation temperature. The actual $\chi_{EX}-T$ behavior is shown in Fig. 10, where $(T/N_A^{EX}) \propto \chi_{EX}^{-1}$ is plotted versus T for three (111)Si/SiO_2 samples of different EX ESR intensity. The least-squares fits (full lines in Fig. 10), reveal a Curie-Weiss behavior,

$$\chi_{EX} \propto \frac{N_{EX}}{T-\Theta_{EX}} , \tag{5}$$

where the characteristic temperature $\Theta_{EX}=2.0\pm0.8$ K

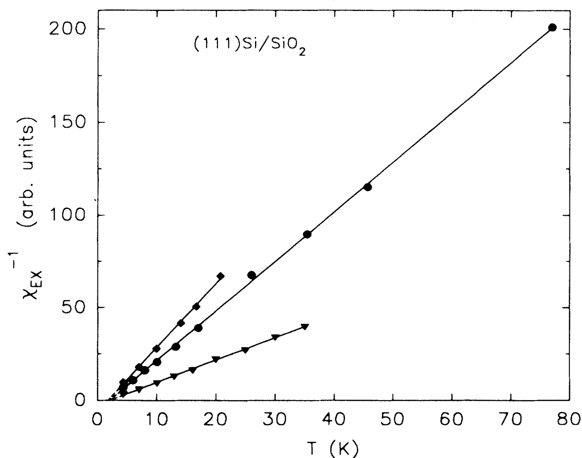

FIG. 10. Inverse EX susceptibility as a function of temperature, measured on three (111)Si/SiO_2 samples grown at 800 °C in 110-kPa dry O_2, exhibiting $N_A^{EX} \approx 0.4$ (diamonds), 0.6 (circles), and 1.2×10^{12} cm^{-2} (triangles) at 4.3 K. The full lines represent linear least-squares fit to the data, from where the characteristic temperature $\Theta_{EX}=2.0\pm0.8$ is inferred, which indicates slight ferromagnetic coupling between the EX spins.

(practically independent of N_A^{EX}), indicating a weak ferromagnetic coupling of the EX spins. (The error bars on Θ_{EX} reflect a relative error of $\pm 20\%$ on N_A^{EX}.)

One consequence of this Curie-Weiss behavior of χ_{EX} is that the N_A^{EX} data, as determined along Eq. (4), do not represent the correct areal EX density, except when measured at sufficiently high temperatures ($T \gg \Theta_{EX}$). Equation (5) shows that the deviation depends on T, the correct areal EX density being obtained by multiplying the N_A^{EX} values "measured" along Eq. (4) by $(T-\Theta_{EX})/T$. The ESR analysis of the EX enter, however, is little affected by this experimental fact.

IV. DISCUSSION: COMPARISON OF *EX* WITH KNOWN DEFECTS

Having described the EX defect's generation characteristics[16] and its salient ESR features, it remains, of course, to unravel the atomic and electronic nature of the (ESR-active) EX defect entity. Important features that should be kept in mind when addressing this question include (1) the defect's isotropic g tensor (Sec. III B), (2) the isotropic symmetric 16.1-G ^{29}Si hf doublet (Sec. III C) flanking the central ESR signal, (3) its location in the top 40 Å of the SiO_2 layer (regardless of d_{ox}), and (4) the fact that the EX center is inherent to the SiO_2 growth process. It is investigated below whether the EX features come anywhere close to the characteristics of known defects in Si/SiO_2, or if they relate to properties of other isotropic signals reported in the literature.

First, according to the analysis in Sec. III C, an impurity-related origin for the EX defect can be ruled out on the ground of the ^{29}Si hf doublet properties. This excludes, for instance, the populated ^{31}P donors in Si and all N-related defects such as, e.g., the fourfold Si-coordinated N atom.[37] Further, all defects located in the Si substrate or at the Si/SiO_2 interface (the P_b centers) cannot be kept as valuable candidates. Neither can defects that exhibit a *measurable* g tensor anisotropy: in particular, all intrinsic ($\equiv$ not impurity-related) defects so far identified in SiO_2 may be discarded, simply on the basis of their g anisotropy. These centers include all variants of E' [E'_α, E'_β, E'_γ (Ref. 23) and E'_δ (Ref. 24)], the so-called "wet" and "dry" oxygen hole centers—that is, the nonbridging oxygen hole center (NBOHC) and the peroxy radical[38]—and the self-trapped holes.[39] Among all these centers, the one that comes closest to the EX defect is E'_δ, a variant of E' introduced in synthetic silica (prepared by plasma oxidation of $SiCl_4$) of low OH content (≤ 10 ppm) and ~ 4000 ppm Cl impurities after 100-keV x-ray irradiation. This center,[24] however, still exhibits some g anisotropy ($g_1=2.0018$, $g_2=g_3=2.0021$), which makes it well distinct from the EX defect.

Apart from the above-mentioned well-characterized defects in SiO_2, there have additionally been reported several observations of isotropic resonances associated with Si or Si/SiO_2 with g values close to g_{EX}. Müller *et al.*[40] found, in a study of the properties of clean Si surfaces, that when heating Si, crushed in ultrahigh vacuum, to $T \sim 380-400$ °C in an ambient containing oxygen, a

narrow resonance at $g = 2.0029$ appeared in addition to the dangling bond line at $g = 2.0055$. Heating Si crushed in air to 400–700 °C in a moderate vacuum caused the appearance of another narrow ($\Delta B_{pp} \approx 0.8$ G) resonance at $g = 2.0024$, previously observed by Kusumoto and Shoji[41] and attributed to broken surface bonds. While Müller *et al.* associated this line with dissolved oxygen coming to the Si surface, Chung and Haneman[42] believed the signal to originate from some variable impurity contamination. There have been various reports in the literature of narrow signals of $g \approx 2.0027$ and $\Delta B_{pp} \approx 1$ G from surfaces of several semiconductors or glasses after heat treatment.[43,44] The signals are generated by vacuum heat treatment in the range 400–600 °C. The linewidth broadens significantly when exposing the samples to low O pressure ($\sim 10^{-1}$ Torr) and the signals disappear upon exposure to air at room temperature. They also are permanently eliminated by heating at ~750 °C. These kind of universal signals have been shown to arise from carbon surface contamination from the vacuum system and are attributed to unpaired electrons stabilized as free radicals in aromatic C-ring structures on the surfaces of these solids. It is clear, however, that the outlined properties of the stable *EX* defect show no relationship with these defects.

Griscom and co-workers[45] have observed narrow resonances when studying SiO_2 glasses annealed in evacuated silica tubes at elevated temperatures: In optical fibers with a Suprasil core, they observe an isotropic singlet of $g \sim 2.0022$ and $\Delta B_{pp} = 3$–4 G after heat treatment *in vacuo* or in an inert or reducing atmosphere. In P_2O_5-SiO_2 glass, they observe an isotropic signal characterized by $g \sim 2.0030$ and $\Delta B_{pp} \sim 2.6$ G, denoted as *S* center. However, these signals were found to disappear upon heat treatment in oxidizing atmosphere above ~430 °C. The latter behavior, which is much reminiscent of the above-mentioned universal type of surface defect, conflicts with the *EX* properties. In a tentative explanation, these authors have assigned the signal to *E'*-type defects of the type $(OSi_2)\equiv Si^{\bullet}$ and/or $(O_2Si)\equiv Si^{\bullet}$.

Isotropic resonances were also observed in thermally oxidized *c*-Si. Besides a broad resonance at $g = 2.0029$, Brower[46] found a narrow (0.7 G) Lorentzian line at $g = 2.0026$ (termed *SL*8) in Si/SiO_2 thermally grown at ~1050 °C for 30 min in dry O_2 (resulting in $d_{ox} \approx 500$ Å). The signal was associated with the thermal oxide but no decisive explanation as to its origin could be delineated: Its appearance could be related to contamination during the high-*T* oxidation or be caused by a surface-related defect. Previously, Brower reported the observation of a single isotropic resonance of $g = 2.0028$ and $\Delta B_{pp} \approx 2$ G in *c*-Si implanted with $\sim 10^{15}$ 200-keV $^{14}N^{+}$ cm^{-2} and subsequently annealed at 800 °C, but this line was very likely related to N.[47]

For various reasons, none of these signals appears related to the *EX* defect. Fist, some of them are only generated in an appreciable intensity in a temperature range far below (<600°C) or above (>1000 °C) the range in which *EX* centers are grown in substantial amounts, or in another oxide thickness range (>500 Å). Second, exposure to oxygen during annealing removes some of the signals observed in heated crushed Si, whereas the *EX* defect is grown in during thermal oxidation (i.e., in O_2 ambient). Finally, none of the reported signals are accompanied by any observable hf structure, unlike the *EX* center.

In a final step, one may consider the possibility that the *EX* signal arises from overcoordinated or undercoordinated oxygen. Lucovsky has argued[48] that the C_3^{+1} and C_1^{-1} defects (the positively charged threefold coordinated O atom and the negatively charged undercoordinated O atom in the notation of Kastner, Adler, and Fritzsche[49]) can occur as near neighbors in the SiO_2 network termed intimate valence-alternation pairs. Dianov *et al.*[50] investigated the threefold coordinated O complex in three charge states ($-1e, 0e, +1e$) using a minimal cluster approach. According to their calculations, C_3^{+1} yields the most stable configuration, while C_3^0 (with ~3.8 eV higher formation energy) is the only spin-active entity. When C_3^{+1} transforms into C_3^0 through trapping of an electron, it would become a sort of neutral *E'* center. On the basis of the known *g*-tensor asymmetry, the C_3^0 defect may thus also be excluded as the origin of the *EX* center. A similar argument holds for the spin active C_1^0 state: when C_1^{-1} transforms into C_1^0 through trapping of a hole, it would become a neutral NBOHC.

This discussion shows that, based on its particular ESR features, the *EX* defect does not fit into one or the other class of presently known extrinsic or intrinsic defects in *a*-SiO_2 (more specifically, in thermal SiO_2 on Si).

V. SUMMARY

We have presented an ESR analysis of the natural intrinsic *EX* defect in thermal SiO_2 on Si. Its salient ESR features, such as *g* factor, areal density, linewidth, the Voigt-like line shape, and the hyperfine structure are identical for both (111) and (001)Si/SiO_2.

The Voigt-like line shape of the central *EX* signal has been consistently deconvoluted . It is found to result from a residual Gaussian component and a Lorentzian part, mainly originating from magnetic dipole-dipole interaction between *EX* spins, which increases linearly with *EX* concentration; for low *EX* densities (i.e., $N_A^{EX} \rightarrow 0$), a Lorentzian small component of $\Delta B_{pp}^{L} \sim 0.26$ G of different origin remains. The theoretical predictions of dipolar broadening in the low fractional population limit, starting from the measured *EX* densities, comply with observations. The residual Gaussian part ($\Delta B_{pp}^{G} \approx 0.80$ G at 800 °C) may arise from a weak spread in the *EX g* value (glass effect) and/or inhomogeneous broadening originating from unresolved hyperfine interaction. It is found to depend weakly on oxidation temperature, where it is seen to narrow from $\Delta B_{pp}^{G} \approx 0.80$ G at $T_{ox} = 800°$ to ≈ 0.64 G at $T_{ox} = 930$ °C. This is correlated with the structural relaxation of the superficial SiO_2 layer that the defects reside in, setting in from ~850 °C onwards. This interpretation then would rather be in favor of a glass effect origin of the Gaussian portion of the broadening.

Neither the *g* value nor the linewidth showed any significant *T* dependence in the range 4.3–77 K, while the *EX* susceptibility behaves Curie-Weiss-like indicating a weak ferromagnetic coupling of the *EX* spins at low *T*

characterized by the temperature $\Theta_{EX} \sim 2$ K.

The symmetric isotropic 16.1-G doublet centered at the central *EX* line is ascribed to ^{29}Si hf interaction of the unpaired spin with three (maybe four) equivalent Si sites, which are not the defect's prime "core" atoms according to the magnitude of the hf splitting, but rather first- or higher-order nearest neighbors. The *EX* center appears not impurity related and does not belong to any family of presently known intrinsic defects in a-SiO_2, neither can its ESR signal be identified with other isotropic resonances reported in the literature. Overcoordinated or undercoordinated oxygen is also excluded as the source of the *EX* signal.

The *EX* ESR features rather point to an unpaired spin occupying an effectively highly *s*-like orbital delocalized over several atomic sites, and which has a superhyperfine interaction with three (perhaps four) equivalent neighboring Si sites. Further research must involve isotopical enrichment to reveal the core of the *EX* defect structure.

ACKNOWLEDGMENT

Support of this work by the Belgian National Fund for Scientific Research is gratefully acknowledged.

[1]R. A. Weeks, J. Appl. Phys. **27**, 1376 (1956).
[2]D. L. Griscom, E. J. Friebele, and G. H. Sigel, Jr., Solid State Commun. **15**, 479 (1974).
[3]D. L. Griscom, Phys. Rev. B **20**, 1823 (1979); **22**, 4192 (1980).
[4]F. J. Feigl, W. B. Fowler, and K. L. Yip, Solid State Commun. **14**, 225 (1974).
[5]K. L. Yip and W. B. Fowler, Phys. Rev. B **11**, 2327 (1975).
[6]Y. Nishi, Jpn. J. Appl. Phys. **10**, 52 (1971).
[7]E. H. Poindexter and P. J. Caplan, Prog. Surf. Sci. **14**, 211 (1983).
[8]A. Stesmans, Phys. Rev. B **48**, 2418 (1993).
[9]P. J. Caplan, E. H. Poindexter, B. E. Deal, and R. R. Razouk, J. Appl. Phys. **50**, 5847 (1979); **52**, 879 (1981).
[10]K. L. Brower, Appl. Phys. Lett. **43**, 1111 (1983).
[11]A. Stesmans, Appl. Phys. Lett. **48**, 972 (1986).
[12]A. H. Edwards, Phys. Rev. B **36**, 9638 (1987).
[13]M. Cook and C. T. White, Phys. Rev. Lett. **59**, 1741 (1987).
[14]A. Stesmans, Phys. Rev. B **45**, 9501 (1992).
[15]The center is new in the sense that the authors are unaware of any previous ESR report (see, also, Sec. IV). It is possible, however, that the defect has been detected before as a charge trap by electrical measurements.
[16]A. Stesmans and F. Scheerlinck, J. Appl. Phys. **75**, 1047 (1994).
[17]M. Grundner, D. Graf, P. O. Hahn, and A. Schnegg, Solid State Technol. **34**, 69 (1991).
[18]See, e.g., M. Grundner and H. Jacob, Appl. Phys. A **39**, 73 (1986).
[19]G. Van Gorp and A. Stesmans, Phys. Rev. B **45**, 4344 (1992); G. Van Gorp, Ph.D. thesis Katholieke Universiteit Leuven, 1991.
[20]A. Stesmans, J. Mag. Reson. **76**, 14 (1988).
[21]To minimize interference of the *EX* resonance with the unavoidably copresent P_b signal, the preferred field direction is $\mathbf{B}\perp[111]$ when studying (111)Si/SiO_2 samples. For (001)Si/SiO_2 structures, however, the optimum choice is $\mathbf{B}\|[001]$.
[22]A. Stesmans, J. Braet, J. Witters, and R. F. Dekeersmaecker, Surf. Sci. **141**, 255 (1984).
[23]D. L. Griscom, Nucl. Instrum. Methods Phys. Res. B **1**, 481 (1984).
[24]D. L. Griscom and E. J. Friebele, Phys. Rev. B **34**, 7524 (1986).
[25]D. W. Posener, Aust. J. Phys. **12**, 184 (1959).
[26]C. Kittel and E. Abrahams, Phys. Rev. **90**, 238 (1953).
[27]See, e.g., D. L. Griscom, Glass Sci. Technol. **4B**, 151 (1990).
[28]J. H. Van Vleck, Phys. Rev. **74**, 1168 (1948).
[29]S. J. Wyard, Proc. Phys. Soc. **86**, 587 (1965).
[30]The DD linewidth pertaining to *EX* DD interaction is just obtained by subtracting the remaining Lorentzian portion of 0.26 G, as the linewidth of a convolution of two Lorentzian shapes is simply the sum of the linewidths of the constituents.
[31]*Handbook of Chemistry and Physics,* edited by R. C. Weast (Chemical Rubber, Cleveland, 1971).
[32]Other discrimination between either $I=1$ or $I=\frac{1}{2}$ hf interaction could come from the observation of the eventual second-order hf shift (see, e.g., Ref. 33). For the observed splitting $a=16.1$ G, however, such a shift would only amount to ~ 10 mG, which, unfortunately, is experimentally inaccessible.
[33]See, e.g., G.E. Pake and T. L. Estle, *The Physical Principles of Electron Paramagnetic Resonance* (Benjamin, London, 1973).
[34]P. W. Atkins and M. C. R. Symons, *The Structure of Inorganic Radicals* (Elsevier, Amsterdam, 1967).
[35]Trade name of Heraeus, Inc.
[36]T. G. Castner, Jr., Phys. Rev. **115**, 1506 (1959).
[37]T. E. Tsai, D. L. Griscom, and E. J. Friebele, Phys. Rev. B **38**, 2140 (1988).
[38]M. Stapelbroek, D. L. Griscom, E. J. Friebele, and G. H. Sigel, Jr., J. Non-Cryst. Solids **32**, 313 (1979).
[39]D. L. Griscom, J. Non-Cryst. Solids **149**, 137 (1992).
[40]K. A. Müller, P. Chan, R. Kleiner, D. W. Ovenall, and M. J. Sparnaay, J. Appl. Phys. **35**, 2254 (1964).
[41]H. Kusumoto and M. Shoji, J. Phys. Soc. Jpn. **17**, 1678 (1962).
[42]M. F. Chung and D. Haneman, J. Appl. Phys. **37**, 1879 (1966).
[43]P. Chan and A. Steinemann, Surf. Sci. **5**, 267 (1966).
[44]D. J. Miller and D. Haneman, Surf. Sci. **24**, 639 (1971).
[45]D. L. Griscom, E. J. Friebele, K. J. Long, and J. W. Fleming, J. Appl. Phys. **54**, 3743 (1983); E. J. Freibele, G. H. Sigel, Jr., and D. L. Griscom, Appl. Phys. Lett. **28**, 516 (1976).
[46]K. L. Brower, in *SiO_2 and Its Interfaces,* edited by S. T. Pantelides and G. Lucovsky, MRS Symposia Proceedings No. 105 (Materials Research Society, Pittsburgh, 1988), p. 219.
[47]K. L. Brower, Phys. Rev. B **26**, 6040 (1982).
[48]G. Lucovsky, Philos. Mag. B **39**, 531 (1979).
[49]M. Kastner, D. Adler, and H. Fritzsche, Phys. Rev. Lett. **37**, 1504 (1976).
[50]E. M. Dianov, A. V. Egibyan, S. A. Akopyan, A. E. Rustamyan, V. O. Sokolov, and V. B. Sulimov, Phys. Status Solidi B **161**, 55 (1990).